Ceramide Levels and COVID-19 Respiratory Distress, a Causal Relationship

Mehran Khodadoust (mehran@vexopharma.com)
Vexo Pharmaceuticals DMCC

Research Article

Keywords: plasma ceramide concentration, respiratory distress symptoms, COVID-19

Posted Date: May 12th, 2021

DOI: https://doi.org/10.21203/rs.3.rs-443020/v3

Title: Ceramide Levels and COVID-19 Respiratory Distress, a Causal Relationship

Author: Mehran M. Khodadoust*

Affiliations:

*Vexo Pharmaceuticals, DMCC; Dubai, UAE.

Corresponding author. Email: Mehran@vexopharma.com

One Sentence Summary: Ceramide-dependent lipotoxicity in COVID-19-associated respiratory distress, a method for diagnosis and treatment.

Abstract: A causal relationship between plasma ceramide concentration and respiratory distress symptoms in COVID-19 patients is presented. In this study, plasma samples of 52 individuals infected with COVID-19 were utilized in a lipidomic analysis. Lipids belonging to the ceramide class exhibited a 400-fold increase in total plasma concentration in infected patients. Further analysis led to the demonstration of concentration dependency for severe COVID-19 respiratory symptoms in a subclass of ceramides. The subclasses Cer(d18:0/24:1), Cer(d18:1/24:1), and Cer(d18:1/22:0) were shown to be increased by 48-, 40-, and 33-fold, respectively, in infected plasma samples and to 116-, 91- and 50-fold, respectively, in plasma samples with respiratory distress. Hence, monitoring plasma ceramide concentration, targeting ceramide synthesis, its salvage and its regulatory mechanisms are validated approaches towards enhancing survival from COVID-19 respiratory distress.

Main Text:

INTRODUCTION

The COVID-19 virus penetrates vital organs such as the lung with a range from asymptomatic or mild infections restricted to the upper respiratory tract to severe respiratory syndromes hallmarked by disseminated spread to the lower airways. Observation of local inflammation and pneumonia, especially in patients with preconditions such as diabetes, hypertension, and cardiovascular disease, has also been reported (*1)*. Supportive supplemental therapy for alleviation of these respiratory distress symptoms is the most viable strategy and the goal of most current efforts for improving COVID-19 patient survival.

Recent studies have highlighted that after infection, some viruses can highjack and utilize host lipid metabolism for their own propagation to counteract the cellular response (*11,12*). To explore evidence for similar virus host exchanges and to better understand the mechanisms by which COVID-19 infects host cells, a number of metabolomics studies have been reported (*2-9)*.

Schwarz et al. described the progression from moderate to severe disease to be marked by loss of specific immune regulatory lipid mediators (LMs) and increased proinflammatory constituents (*3)*. Similarly, Wu et al. reported that in addition to dyslipidemia, major changes to

carbamoyl phosphate and guanosine monophosphate (GMP) levels are also associated with the progression and severity of COVID-19 (*4*). Shen et al., in a metabolomics and proteomic study, revealed characteristic protein and metabolite changes in the sera of severe COVID-19 patients, which might be used in the selection of potential biomarkers for the evaluation of the severity of disease (*5*). All these studies have reported unbiased analyses of patient plasma samples, and all have shown that changes in the Lipidome are associated with severe COVID-19 infection.

In an attempt to further explore changes in patient plasma metabolites as well as in the lipidome upon infection with COVID-19, we utilized a lipidomics approach. We confirmed the association of distinct lipids and tested their modulation in relation to the severity of the infection. Our findings have demonstrated that COVID-19 infection causes modulation of the ceramide (Cer) balance in the host plasma. A concentration-dependent association between increases in subclasses of ceramides and the onset of respiratory distress symptoms of COVID-19 infection was observed.

Ceramides (Cer) are the products of the metabolism of fats and lipids. They have been reported to accumulate in humans with obesity and hyperlipidemia. They are the central metabolites of the sphingolipid family and have also been reported to be signaling molecules that can regulate ER stress, apoptosis, insulin sensitivity and inflammation (*13, 15*). Increased Cer levels are heavily implicated in the pathogenesis of insulin resistance, neurodegeneration conditions, and lung diseases, including asthma, chronic obstructive pulmonary disease (POD), and pulmonary fibrosis (*16*).

Our observations of association and concentration dependency in combination with the current understanding of Cer and their role in the pathobiology of lung inflammation provide reasonable support for defining Cer and COVID-19 infection-mediated respiratory distress as a causal type relationship. By gaining a greater understanding of this relationship, we shed light on the possible treatment options for which further research is needed.

RESULTS

Subhead 1: Identification of differential metabolites

The ions corresponding to d7-androstenedione, d4-cortisol, and d5-DHEAS, used as internal standards, were selected for extraction of the ion chromatographic peaks in an LC/MS/MS-based comparative metabolomics analysis.

Figure 1a shows the obtained score plots from metabolomics profiles of plasma from the COVID-19-infected and control uninfected groups. The clear separation shows that significantly different metabolites are present within each group. The loading plots shown in Figure 1b demonstrate these differences at the component level. The ions that are furthest from the origin of the plots are the ones that make the most contribution to the separation seen in the score plots and were selected for further analysis. Figure 1c shows a profile of a metabolite chosen from the loading plot.

Each component of the loading plot was investigated, and a list composed of the m/z of selected ions with a define profile of abundance and characteristics was formed. Accurate

molecular ion masses were used for composition, calculation, and collection of data-dependent MS/MS data. MS/MS data were collected for structural deduction and database searches.

Subhead 2: Identification and structural deduction of metabolites via data-dependent MS/MS

Figure 2 shows an overview of the results from the analysis of plasma from uninfected and COVID-19-infected individuals using a data-dependent MS/MS method. The combined monitored m/z ion profile from this analysis confirms the principal component analysis (PCA)-directed selection process. Structural deduction and database searches demonstrate that >283 of the metabolites identified belong to the lipid family.

Subhead 3: From metabolomics to lipidomics

Figure 3a shows the identification, categorization and quantification of identified lipid metabolites: PS = Phosphatidylserine, Cer = Ceramides, PE = Phosphatidylethanolamine, PI = Phosphatidylinositol, PG = Prostaglandin, HexCer = Hexosylceramide, Hex2Cer = DiHexosylceramide, Hex3Cer = TriHexosylceramide by using the combination of obtained peak list of selective ions, obtained MS/MS data, and LIPID CREATOR platform(*10*). Figure 3b shows the observed retention time (RT) differences between the identified metabolites in the plasma of uninfected and COVID-19-infected individuals. A change in RT in components of each class reflects changes in the subclasses of the lipids in each class.

The changes in levels of each lipid class can be represented by showing the average fold sum of median of means (MEDM) changes in the peak area of each identified lipid subclass in that class relative to the uninfected. Figure 4a shows the changes in the number of lipid subclasses observed in the plasma due to COVID-19 infection with mild symptoms compared to the uninfected candidates, in addition to the average fold sum of MEDM changes per class. Figure 4b also shows the changes in the number of subclasses of lipids per class in the plasma of individuals infected with COVID-19 with respiratory distress symptoms in comparison to the uninfected group, in addition to the average fold sum of MEDM changes per lipid class. Figure 4c demonstrates the changes in the average fold sum of MEDM and the number of subclasses of each of the lipid classes in the plasma of the patients with COVID-19 infected with mild symptoms vs infected with respiratory distress symptoms.

In the plasma samples from COVID-19 patients with mild symptoms (Figure 4a) and patients with respiratory distress symptoms (Figure 4b), an average 40-fold increase in the concentration of lipid classes Cer, HexCer, Hex2Cer, Hex3Cer, PG, and PS was observed. Figure 4c shows that when only comparing the metabolic differences in the plasma of the Covid-19 infected with mild to the severe symptoms, the observed changes in lipid profiles become limited to Cer (average more than 1.5 - 2 fold increase this study) and its derivatives HexCer, Hex2Cer.

Subhead 4: Covid-19 respiratory distress and Cer

The compositional makeup of the subclasses of lipids present in the plasma of COVID-19-infected patients with mild symptoms vs those with respiratory distress shows no change at the subclass levels in each class of the identified lipids (Supplementary Figure 1). The overall change in plasma concentration of each lipid class is estimated by multiplying the average fold increases in peak area of each subclass by the number of identified lipid subclasses. Figure 5a demonstrates the concentration of each lipid class in relative terms of fold induction to the

uninfected control group. Figure 5b shows the calculated plasma concentration of Cer and Sphingomyelin (SM) class of lipids in µmol/l in the uninfected, infected with mild, and infected with severe respiratory distress symptoms (SRM 1950 – metabolites by LIPID MAPS consortium, was the basis for comparison and establishment of concentration (*14*)). SM, which is not modulated in plasma by COVID-19 infection, serves as a control in this study. These figures show that the total levels of Cer are increased in the plasma of COVID-19-infected individuals with mild symptoms by more than 250-fold or 500 µmol/l. In cases of COVID-19-infected individuals with severe respiratory distress symptoms, Cer levels were increased by over 450-fold or 720 µmol/l (Figure 5a, 5b). In summary, an increase in 220 µmol/l plasma Cer concentration is the change seen between a COVID-19 infection with mild symptoms and an infection with a severe respiratory distress response.

Figure 6a shows breaking down the increases in plasma Cer concentration back into subclass levels. This figure shows the relative contribution of each of the Cer subclasses in terms of fold increases in plasma concentration compared to the uninfected and mild vs respiratory distress patients. This figure shows a range of 20- to 160-fold increases relative to the uninfected group in the concentrations of Cer(d18:0/24:1), Cer(d18:1/24:1), Cer(d18.0/20:0), and Cer(d18:1/20:0) in the plasma of mild and respiratory distress patients. Figure 6b shows a comparative measurement of the concentration of the Cer subclasses in plasma in µmol/l, as related to Covid-19 infection (SRM 1950 – metabolites by LIPID MAPS consortium was the basis for comparison and establishment of concentration (*14)*). The overall levels of Cer(d18:1/16:0) were 2.79 µmol/l, Cer(d18:1/24:1) was 39.57 µmol/l in the plasma of COVID-19-infected individuals with no symptoms of distress, Cer(d18:1/16:0) was increased to 3.63 µmol/l (30% increase), and Cer(d18:1/24:1) was increased to 95.63 µmol/l (142% increase) in the plasma of respiratory distress individuals.

Ratios of lipids can be a very informative tool for the process of identifying more selective targets for the regulation of each Cer subclass. Figure 6c and 6d show comparative ratios of the identified subclasses Cer with their associated dihydroceramide and monohexosylceramide species in the plasma of COVID-19-infected individuals with mild vs severe respiratory distress symptoms. These figures demonstrate both the presence and relative ratio of the Cer substrates to Cer in a subclass-dependent manner. In figure 6c, the almost 2-fold greater Cer(18:1/22:0) to its hexosyl derivative ratio in respiratory distress patients shows a tool to predict severe respiratory distress and a possible mechanism for modulation. Figure 6d demonstrates the relative abundance of substrates for de novo synthesis of Cer(d18:1/20:0), Cer(d18:1/16:0), and Cer(d18:1/24:1) in the plasma of COVID-19-infected individuals.

DISCUSSION

A causal relationship between plasma levels of Cer and the onset of COVID-19 respiratory distress symptoms is claimed. Cer involvement has been highlighted in reports of lung diseases, including acute lung injury, cystic fibrosis, emphysema, lung infections, and asthma (*13,16*). These reports show pulmonary manifestations to be the main symptoms of Cer-mediated toxicity. Cers can regulate major aspects of lung endothelial cell function and are involved in the pathogenesis of several conditions associated with pulmonary vascular dysfunction (*16*). These pulmonary manifestation symptoms are common with the symptoms also seen in patients with COVID-19-associated respiratory distress (*17*). The reported high

levels of plasma Cer concentration in obese and asthmatic individuals are consistent with the observed sensitivity of this group to COVID-19 infection, supporting its biological relevance (*25*).

In this study, in addition to the described biological relevance, we show association, and concentration dependency of specific subclasses of Cer in the plasma of COVID-19-infected individuals, with the observed respiratory distress symptoms. These findings provide support for the existence of a causal type relationship.

COVID-19 infection causes profound changes in the metabolome of infected individuals, including plasma lipid levels. In this study, changes in plasma levels of 283 lipids covering 8 lipid classes, including PS, PE, PG, Cer, HexCer, Hex2Cer, and Hex3Cer, were identified to be associated with COVID-19 infection. Figure 3a, 3b shows the levels of subclasses of the above classes, as represented by peak area, to be markedly increased in the plasma of COVID-19-infected individuals, describing an association between the identified subclasses of lipids and COVID-19-infected plasma.

Figure 5a shows changes in the concentration of Cer as a class. In terms of fold induction, the total levels of Cer were increased in the plasma of COVID-19-infected individuals with mild symptoms by more than 250-fold or 500 μmol/l (figure 5b). In cases of COVID-19-infected individuals with severe respiratory distress symptoms, this total Cer level is increased by over 450-fold or 720 μmol/l, demonstrating concentration dependency. In other words, the difference between a COVID-19 infection with mild symptoms and an infection with severe respiratory distress response at the lipid class level is an increase of 220 μmol/l plasma in total Cer class concentration. The predominant Cer subclasses (figure 6a and 6b) detected to be associated with these plasma levels in respiratory distress COVID-19 infection were Cer(d18:1/16:0) at 3.63 μmol/l and Cer(d18:1/24:1) at 95.63 μmol/l. The concentrations were 2.79 μmol/l (30% less) and 39.57 μmol/l (142% less), respectively, in the plasma of COVID-19-infected individuals with no symptoms of distress.

The Cer(d18:1/16:0) and Cer(d18:1/24:1) subclasses were reported to be involved in a cardiac mortality study and to be associated with an increased risk of cardiac death outcomes in patients with stable coronary artery disease (*18*). In this study, we report that COVID-19 infection causes a significantly greater mortality risk with a 10- and 30-fold increase in plasma levels of these subclasses over the reported cardiac mortality prediction level.

Causality assessment leads us to believe that monitoring and therapeutic aims of reducing Cer(d18:1/16:0) and Cer(d18:1/24:1) levels in the plasma of patients are required to enhance survival from COVID-19 respiratory distress. A reduction in plasma levels of the above Cer subclasses (bringing down the observed plasma levels to the level seen associated with mild symptoms) can be an aid in the recovery process of the severe symptoms associated with Covid-19 infection.

Cer is generated by de novo synthesis, salvage of sphingosine, and breakdown of complex sphingolipids, including sphingomyelin. The necessary substrates are monohexocylceramide, sphingomyelin, and dihydroceramide (*20*). An increase in all three of these substrates was observed in the plasma of COVID-19-infected individuals (figure 3a, figures 6a, and 6b).

To effectively modulate the toxic effects of Cer in the context of COVID-19 infection is to reduce its circulating concentrations. This can be achieved by inhibiting its biosynthesis or by chemical modification of the circulating Cer in the plasma. The Cer de novo synthesis pathway includes a series of enzymes that produce Cer from the starting components serine and palmitoyl CoA. Researchers seeking to pharmacologically inhibit Cer synthesis in vivo have generally used myriocin, which inhibits serine palmitoyltransferase, the rate limiting initial step in the biosynthesis of all sphingolipids (*20*).

Ceramide synthase (CerS) catalyzes the acylation of the amino group of sphingosine, sphinganine, and other sphingoid bases using acyl CoA esters. CerSs consist of six enzymes (CerS1–6), with each isoform synthesizing a subset of Cer with partially distinct acyl chain lengths. CerS1 forms Cer18, CerS2 forms Cer24, and CerS6 forms Cer16 ceramide (*21*). Since Cer(d18:1/16:0) and Cer(d18:1/24:1) are the predominant subclasses seen in the plasma samples of the COVID-19-infected group, focusing on modulation of CerS2 and CerS6 seems to be the logical therapeutic approach. Inhibitors of the Cers2 enzyme include fumonisins, the related AAL toxin, and australifungins (*22*).

A reduction in the circulating concentration of Cer in the plasma can be achieved by causing chemical modifications with the introduction of enzymes or agonists to at least one ceramide-modifying enzyme, such as glucosylceramide synthase, ceramidase (SMase), ceramide kinase, and sphingomyelin synthase. Both acid and neutral SMase inhibitors, as well as inhibitors of the de novo pathway of Cer synthesis, effectively inhibited Cer-induced apoptosis in the lung in various acute or chronic injury models in vivo, as recently reviewed by Uhlig and Gulbins (*22*). Carpinteiro et al. reported that pharmacological and genetic inhibition of the acid SMase enzyme can prevent infection of cells with COVID-19, VSV and PP. VSV viruses (*21*).

Indirect examples of regulators or circulating Cer levels have also been described to include TNF-alpha inhibitors, TLR-4 inhibitors, adiponectin, FGF21, apoptosis inhibitors, and mitophagy inhibitors (*23, 24*).

Future studies should address more effectively the limitations of this study, the third criterion for causality, which requires alternative explanations for the observed relationship between two variables to be ruled out (nonspuriousness, or “not false.”). To better address these criteria, one would need to directly monitor the effect of lowering plasma concentrations of Cer by treatment with Cer inhibitors on COVID-19-mediated respiratory distress. Furthermore, our investigations have focused on the detected subclasses of Cer isolated through a non-comprehensive metabolomics analysis paradigm, and a more comprehensive approach may lead to the identification of more sensitive subclasses of these lipids.

In summary, uncovering causal relationships is an important first step towards understanding disease and predicting the course of future treatments. In this study, a causal relationship between plasma Cer plasma concentration and respiratory distress symptoms in COVID-19 patients is presented. Specific subclasses of Cer have been identified that can be used for monitoring COVID-19 infection severity and progression. The causality relationship also defines that modulating ceramide synthesis pathways, its salvage and its regulatory mechanisms is a validated approach towards enhancing survival from COVID-19 respiratory distress.

MATERIALS AND METHODS

Materials

Ammonium formate and formic acid were purchased from Sigma Aldrich Chemicals Co. (St. Louis, Mo, USA), LC-MS Grade Methanol, and Optima-grad acetonitrile (ACN) from Fisher Scientific (Pittsburg, PA, USA). A Millipore Milli-Q purification system (Bedford, MA, USA) was used to prepare deionized water. A total of 50 human plasma samples (K3EDTA) from active COVID-19-infected participants (positive via PCR), including 18 with severe respiratory distress and 32 with mild symptoms, were purchased from PRECISION FOR MEDICINE (Norton, MA, USA). All biospecimens have been certified to have been collected under a clinical study that has been reviewed by an institutional/Independent Review Board (IRB) in accordance with the requirements of local governing regulatory agencies, including the DHHS and FDA Codes of Federal Regulations, on the Protection of Human Subjects (45 CFR Part 46 and 21 CFR Part 56, respectively). The participants' age range was 19 – 83 years, with 37 of them being female and 13 males. The NIST Standard Reference Material for Human Plasma (SRM1950) was purchased from Sigma Aldrich Chemicals Co., (St. Louis, Mo, USA).

For the metabolomics evaluation directly before analysis, the samples were thawed on ice. Then, 75 µL of precooled ISP precipitant solution (ClinMass® Steriods in Plasma LC-MS/MS Complete Kit (RECIPE Chemicals + Instruments GmbH, Munich, Germany)) was added to 50 µL of plasma, and the mixture was vortexed for 30 s and left for 10 min before centrifugation at 14,000 rpm for 10 min at 4°C. The supernatant was separated, and 40 µl of it was subjected to metabolite analysis by SCIEX X500R UPLC−QTOF/MS. The ISP contains six internal standards steroids in its panel, including d7-androstenedione, d4- cortisol, d5- DHEAS, d5-11-deoxycortisol, d8-17-hydroxyprogesterone, and d3-testosterone.

Instrumentation

HPLC separation was performed using the SCIEX ExionLC AC system on a Phenomenex: Luna® Omega 3 m Polar C18 100A column. Data were collected on a SCIEX X500R QTOF mass spectrometer with SCIEX OS software: TOF – MS survey scan with Information Dependent Acquisition (IDA) – triggering of up to 16 product ion scans. Data processing was also performed in SCIEX OS software with simultaneous identification and quantification being accomplished in single software (all devices from AB SCIEX, Framingham, U.S.A.).

Forty microliters of the sample was injected for chromatography separation at 30 °C, with a flow rate of 0.8 mL/min, 0.1% formic acid and 2 mM ammonium formate in HPLC water as mobile phase A and HPLC acetonitrile and methanol (50:50) plus 0.1% formic acid and 2 mM ammonium formate as mobile phase B. A 26-min linear gradient was set as follows: 0 min: 2% B, 0-1 min: 2% B, 1–16 min: 98% B, 16–20 min: 98% B. The SCIEX X500R QTOF system with a Turbo V™ source and capable of electrospray ionization (ESI) was used in positive polarity. The ion source temperature was set to 500°C, and the ion source voltage was set to 5500 V. An information-dependent acquisition (IDA) method consisting of a TOF-MS survey (250-1100 Da for 350 msec). The declustering potential (DP) was set to 80V. The collision energy (CE) was set to 10 eV with a collision energy spread (CES) of ± 0 eV. To achieve the

most complete MS/MS coverage, the dynamic background subtraction (DBS) function was activated.

Data processing

MarkerView™ Software 1.3 (SCIEX) was used to process, align, deconvolute, and normalize (sum of total area) the obtained raw data in which the retention time (RT) was from 0.5 min to 26 min. Mass and RT tolerance values were set to 10 ppm and 0.15 minutes. Mass and RT of internal standards used for analysis include d7-androstenedione, d4- cortisol, d5- DHEAS, d5-11-deoxycortisol, d8-17-hydroxyprogesterone, and d3-testosterone introduced via the ISP mixture during sample preparation. Principal component analysis (PCA) was used to visualize the system stability of the system and sample distribution. Orthogonal partial least squares discriminant analysis (OPLS-DA) was used to identify the variables responsible for the discrimination. The system stability (RSD %) of m/z, peak areas and retention times were as follows: 0.02 -0.14%, 0.0003 – 0.0007%, 5.9 – 8.5%).

A list of the intensities for each detected peak was generated using retention time and the mass-to-charge (m/z) ratio data pairs as the parameters for each ion. Manual scanning of the 10,000 spectral features represented by a unique m/z, retention time, and peak area allowed for generation of a list of 670 peaks of interest used for further evaluation. The Formula Finder algorithm was used to identify potential differential metabolites and generate a group of probable formulas on an unknown ion based on the secondary fragment information, mass error, and isotope distribution patterns.

After data preprocessing, the LipidCreator workbench software in Skyline (available at https://lifs.isas.de/lipidcreator) was used for both quantification and qualification of the lipid species present within the plasma samples (*10*).

References and Notes

1. Kaddoura, M. AlIbrahim, M. Hijazi, G et al. COVID-19 Therapeutic Options Under Investigation. Front Pharmacol. 2020 Aug 6;11:1196. doi: 10.3389/fphar.2020.01196. PMID: 32848795; PMCID: PMC7424051.
2. Caterino, M. Gelzo, M. Sol, S. et al. Dysregulation of lipid metabolism and pathological inflammation in patients with COVID-19. Sci Rep. 2021 Feb 3;11(1):2941. doi: 10.1038/s41598-021-82426-7. PMID: 33536486; PMCID: PMC7859398.
3. Schwarz, B. Sharma, L. Roberts, L. et al. Severe SARS-CoV-2 infection in humans is defined by a shift in the serum lipidome resulting in dysregulation of eicosanoid immune mediators medRxiv 2020.07.09.20149849; doi: https://doi.org/10.1101/2020.07.09.20149849

4. Wu D, Shu T, Yang X, et al. Plasma Metabolomic and Lipidomic Alterations Associated with COVID-19. Natl Sci Rev. 2020;nwaa086. Published 2020 Apr 28. doi:10.1093/nsr/nwaa086

5. Shen, B. Yi, X. Sun, Y. et al. Proteomic and Metabolomic Characterization of COVID-19 Patient Sera. Cell. 2020 Jul 9;182(1):59-72.e15. doi: 10.1016/j.cell.2020.05.032. Epub 2020 May 28. PMID: 32492406; PMCID: PMC7254001.

6. Kimhofer, T. Lodge, S. Whiley, L. et al. Integrative Modeling of Quantitative Plasma Lipoprotein, Metabolic, and Amino Acid Data Reveals a Multiorgan Pathological Signature of SARS-CoV-2 Infection. J Proteome Res. 2020;19(11):4442-4454. doi:10.1021/acs.jproteome.0c00519

7. Overmyer, K. Shishkova, E. Miller, I. et al. Large-scale Multi-omic Analysis of COVID-19 Severity. Preprint. medRxiv. 2020;2020.07.17.20156513. Published 2020 Jul 19. doi:10.1101/2020.07.17.20156513

8. Thomas, T. Stefanoni, D. Reisz, J. et al. COVID-19 infection alters kynurenine and fatty acid metabolism, correlating with IL-6 levels and renal status. JCI Insight. 2020 Jul 23;5(14):e140327. doi: 10.1172/jci.insight.140327. PMID: 32559180; PMCID: PMC7453907.

9. Roberts, I. Muelas, M. Taylor, J. et al. Untargeted metabolomics of COVID-19 patient serum reveals potential prognostic markers of both severity and outcome medRxiv 2020.12.09.20246389; doi: https://doi.org/10.1101/2020.12.09.20246389

10. Peng, B. Kopczynski, D. Pratt, B. et al. Lipidcreator workbench to probe the lipidomic landscape. Nature Com. 11, 2057 https://doi.org/10.1038/s41467-020-15960-z (2020).

11. Kyle, J. Burnum-Johnson, K. Wendler, J. et al. Plasma lipidome reveals critical illness and recovery from human Ebola virus disease. Proc Natl Acad Sci U S A. 2019 Feb 26;116(9):3919-3928. doi: 10.1073/pnas.1815356116. Epub 2019 Feb 11. PMID: 30808769; PMCID: PMC6397561.

12. Yan, B. Zou, Z. Chu, H. et al. Lipidomic Profiling Reveals Significant Perturbations of Intracellular Lipid Homeostasis in Enterovirus-Infected Cells. Int J Mol Sci. 2019;20(23):5952. Published 2019 Nov 26. doi:10.3390/ijms20235952

13. Petrache, I. Petrusca, D. Bowler, R. Kamocki, K. Involvement of ceramide in cell death responses in the pulmonary circulation. Proc Am Thorac Soc. 2011 Nov;8(6):492-6. doi: 10.1513/pats.201104-034MW. PMID: 22052925; PMCID: PMC3359077.

14. Lange, M. Fedorova, M. Evaluation of lipid quantification accuracy using HILIC and RPLC MS on the example of NIST® SRM® 1950 metabolites in human plasma. Anal Bioanal Chem. 2020 Jun;412(15):3573-3584. doi: 10.1007/s00216-020-02576-x. Epub 2020 Apr 2. PMID: 32240327; PMCID: PMC7220885.

15. Fugio, L. Coeli-Lacchini, F. Leopoldino, A. Sphingolipids and Mitochondrial Dynamic. Cells. 2020 Mar 1;9(3):581. doi: 10.3390/cells9030581. PMID: 32121501; PMCID: PMC7140523.

16. Ghidoni, R. Caretti, A. Signorelli, P. Role of Sphingolipids in the Pathobiology of Lung Inflammation. Mediators Inflamm. 2015;2015:487508. doi: 10.1155/2015/487508. Epub 2015 Dec 3. PMID: 26770018; PMCID: PMC4681829.

17. Gibson, P. Qin, L. Puah, S. COVID-19 acute respiratory distress syndrome (ARDS): clinical features and differences from typical pre-COVID-19 ARDS. Med J Aust. 2020 Jul;213(2):54-56.e1. doi: 10.5694/mja2.50674. Epub 2020 Jun 22. PMID: 32572965; PMCID: PMC7361309.

18. Laaksonen, R. Ekroos, K. Sysi-Aho, M. et al. Plasma ceramides predict cardiovascular death in patients with stable coronary artery disease and acute coronary syndromes beyond LDL-cholesterol. Eur Heart J. 2016 Jul 1;37(25):1967-76. doi: 10.1093/eurheartj/ehw148. Epub 2016 Apr 28. PMID: 27125947; PMCID: PMC4929378.

19. Bandet, C. Tan-Chen, S. Bourron, O. Le Stunff, H. Hajduch, E. Sphingolipid Metabolism: New Insight into Ceramide-Induced Lipotoxicity in Muscle Cells. Int J Mol Sci. 2019 Jan 23;20(3):479. doi: 10.3390/ijms20030479. PMID: 30678043; PMCID: PMC6387241.

20. Yu, Z. Peng, Q. Huang, Y. Potential therapeutic targets for atherosclerosis in sphingolipid metabolism. Clin Sci (Lond). 2019 Mar 19;133(6):763-776. doi: 10.1042/CS20180911. PMID: 30890654; PMCID: PMC6422862.

21. Carpinteiro, A. Edwards, M. Hoffmann, M. et al. Pharmacological Inhibition of Acid Sphingomyelinase Prevents Uptake of SARS-CoV-2 by Epithelial Cells. Cell Rep Med. 2020 Nov 17; 1(8): 100142. Published online 2020 Oct 29. doi: 10.1016/j.xcrm.2020.100142

22. Uhlig S, Gulbins E. Sphingolipids in the lungs. Am J Respir Crit Care Med. 2008 Dec 1;178(11):1100-14. doi: 10.1164/rccm.200804-595SO. Epub 2008 Aug 28. PMID: 18755926.

23. Gomez-Muñoz, A. Presa, N. Gomez-Larrauri, A. Rivera, I. Trueba, M. Ordoñez, M. Control of inflammatory responses by ceramide, sphingosine 1-phosphate and ceramide 1-phosphate. Prog Lipid Res. 2016 Jan;61:51-62. doi: 10.1016/j.plipres.2015.09.002. Epub 2015 Dec 15. PMID: 26703189.

24. Holland, W. Adams, A. Brozinick, J. et al. An FGF21-adiponectin-ceramide axis controls energy expenditure and insulin action in mice. Cell Metab. 2013 May 7;17(5):790-7. doi: 10.1016/j.cmet.2013.03.019. PMID: 23663742; PMCID: PMC3667496.

25. Chaurasia, B. Summers, S. Ceramides - Lipotoxic Inducers of Metabolic Disorders. Trends Endocrinol Metab. 2015 Oct;26(10):538-550. doi: 10.1016/j.tem.2015.07.006. Erratum in: Trends Endocrinol Metab. 2018 Jan;29(1):66-67. PMID: 26412155.

Acknowledgments: VexO Pharmaceuticals DMCC for support and funding.

Author Contributions: M.K. preformed all experiments and wrote the manuscript.

Funding: VexO Pharmaceuticals DMCC for all funding.

Competing interests: The author declares that U.S. Patent Application No.: 63/160,229 has been filled by the author that covers the reported findings of this manuscript.

Data and materials availability: All data are available in the main text and the supplementary materials. Raw MS data, mzML converted data, interest peak lists, picked and integrated peak areas exported from Skyline and the quantified lipid results tables are available in a public repository.

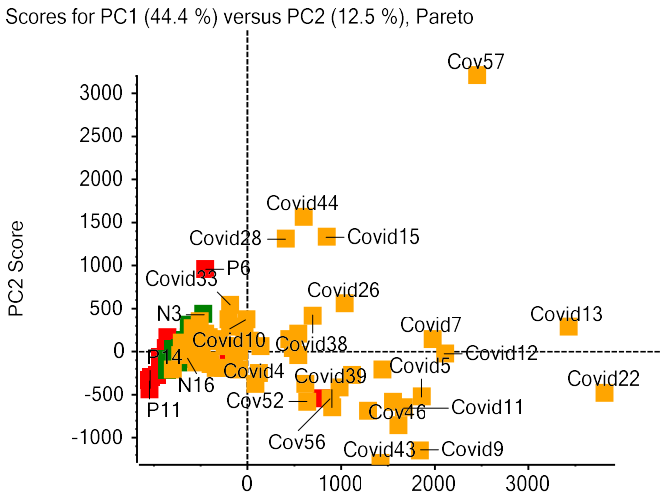

Figure 1 a

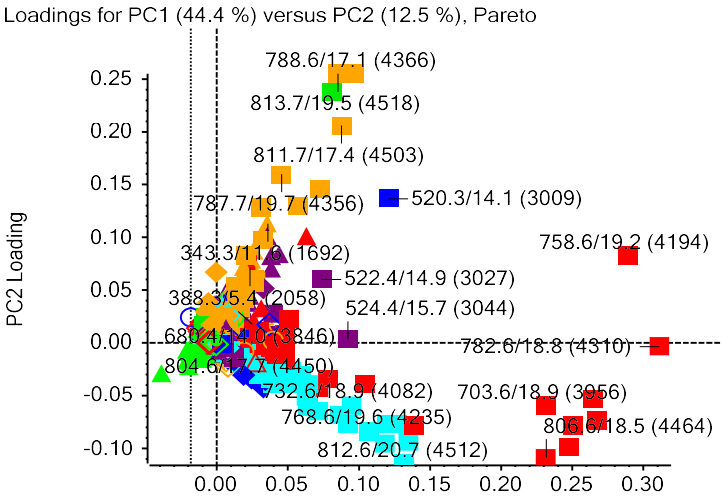

Figure 1 b

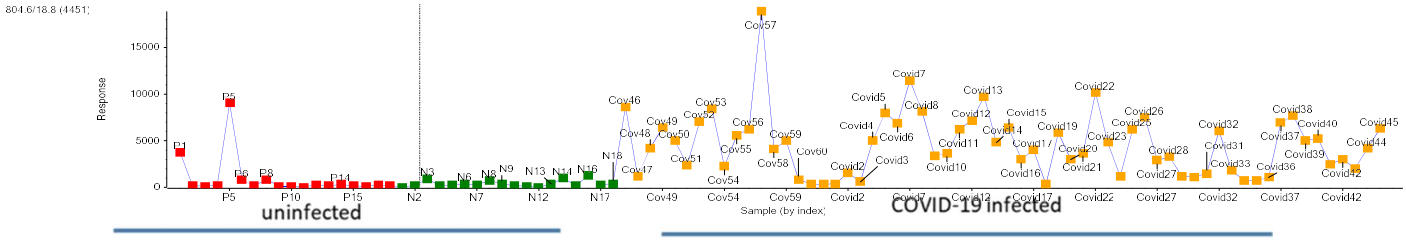

Figure 1 c

Figure 1 . Metabolomics analysis of plasma samples

(A) Scoring and **(B)** loading plots from PCA model analysis of the full-scan MS analysis for classifying COVID-19-infected (yellow squares) and control groups (green squares: noninfected male, red square: noninfected female). **(C)** Example of the peak area profile of a metabolite across samples of COVID-19-infected and control samples, a loading component that drives the observed separation seen between the cohorts by PCA. Using MarkerView [tm] by SCIEX

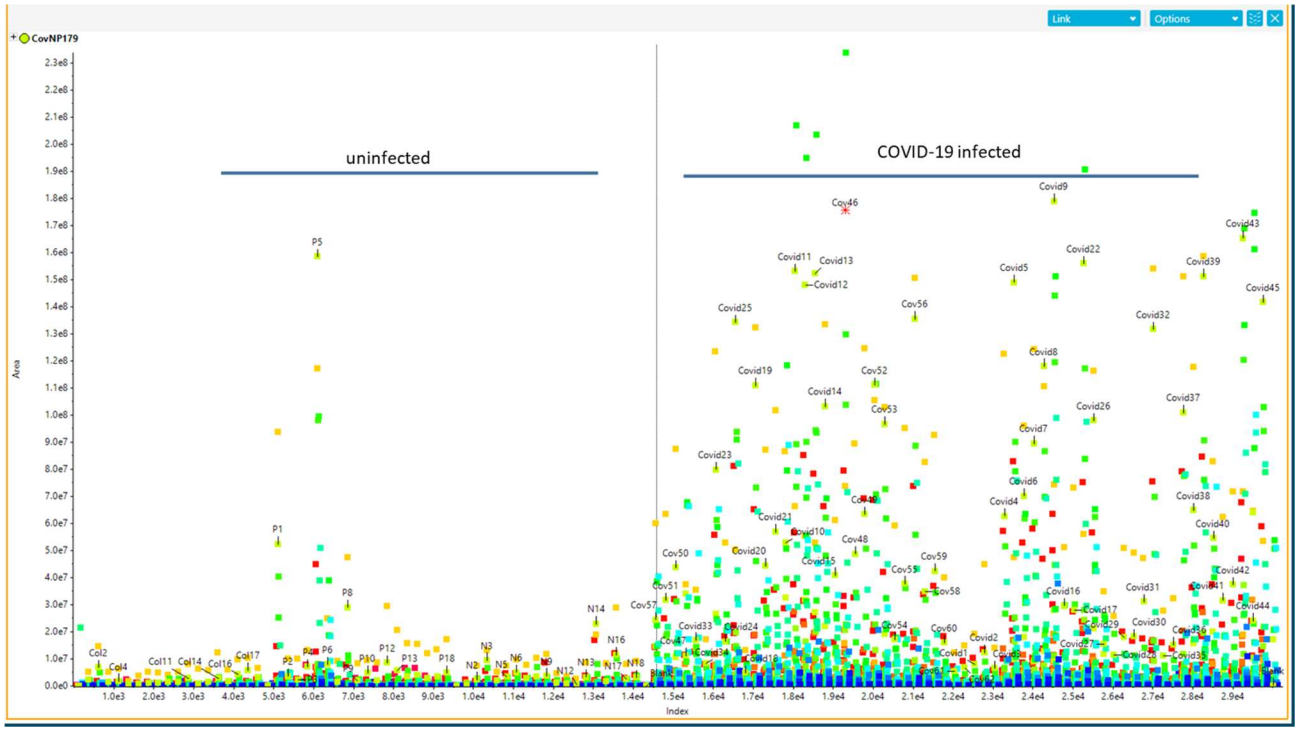

Figure 2. COVID-19 infection and abundance of selected metabolites

LC-MS/MS IDA analysis utilizing the m/z inclusion list provided from the loading component of PCA analysis. The collective representation of the peak area detected for each m/z ion across the analyzed noninfected and COVID-19-infected samples. Each color square represents a metabolite as defined in the inclusion list.

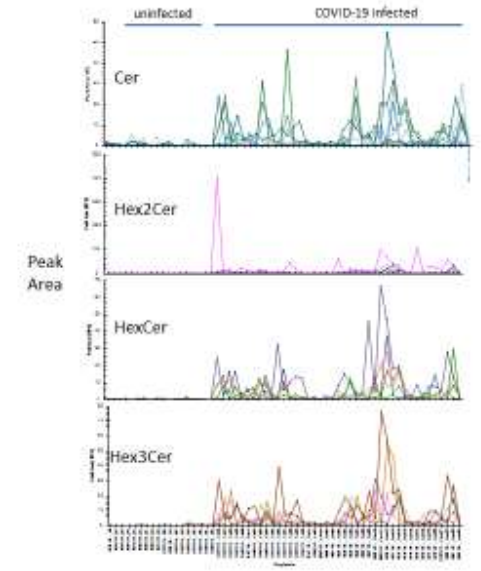

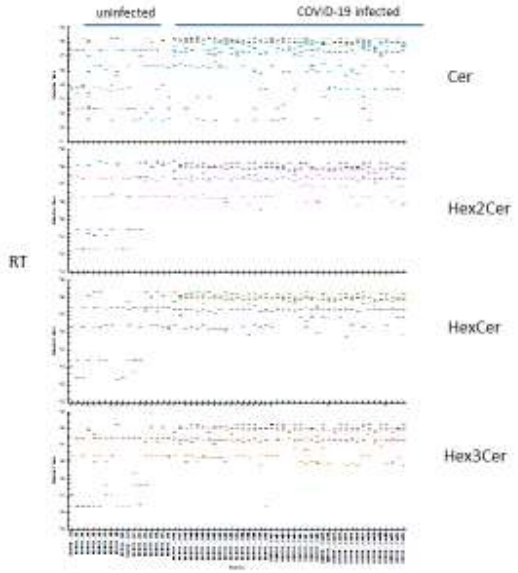

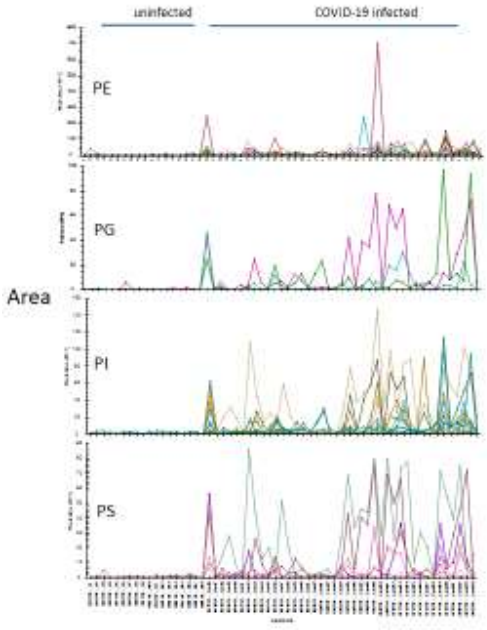

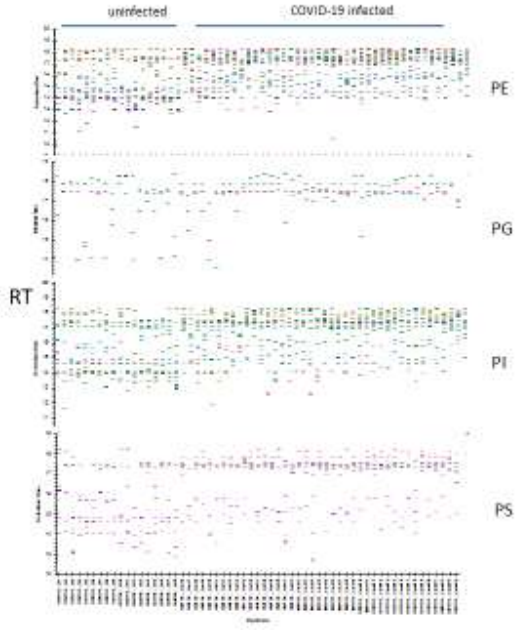

Figure 3a **Figure 3b**

Figure 3. Grouping of identified COVID-19 infection-dependent metabolites into lipid classes

Comparative abundance profile of the identified subclasses of lipids per class in the plasma of uninfected and COVID-19-infected individuals. Segregation, identification and grouping of each identified lipid subclass, in the component list, into lipid classes. **(A)** Observed peak area of components of each class in uninfected and COVID-19-infected plasma samples. **(B)** Observed retention time of each component in each lipid class across all samples. Each metabolite defined in the inclusion list is represented in a different color.

Figure 4a

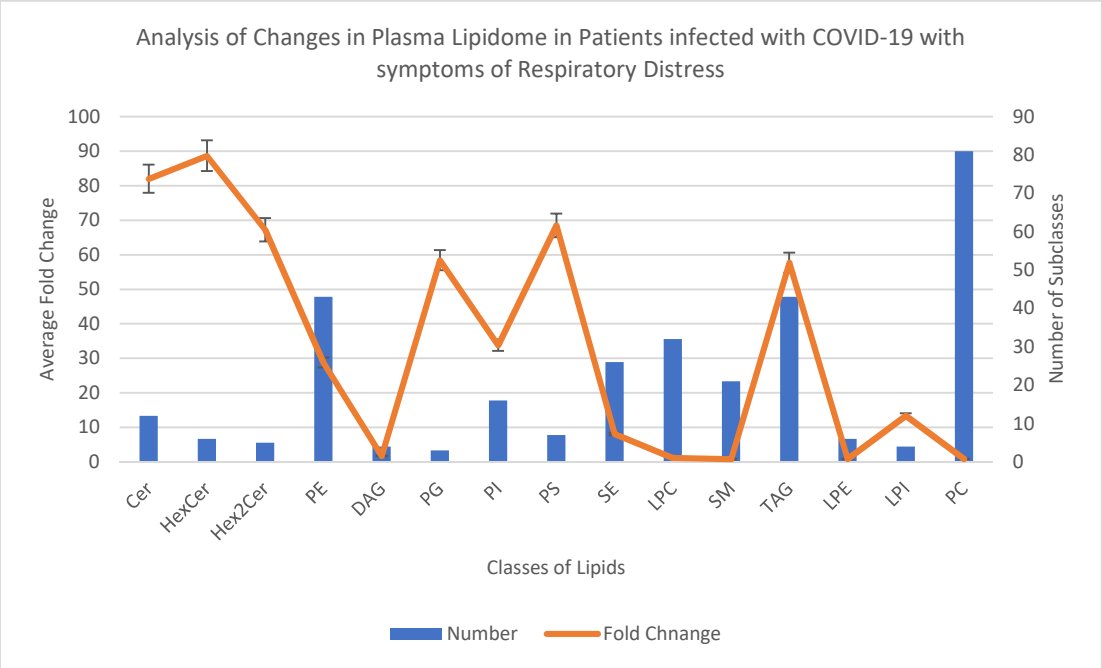

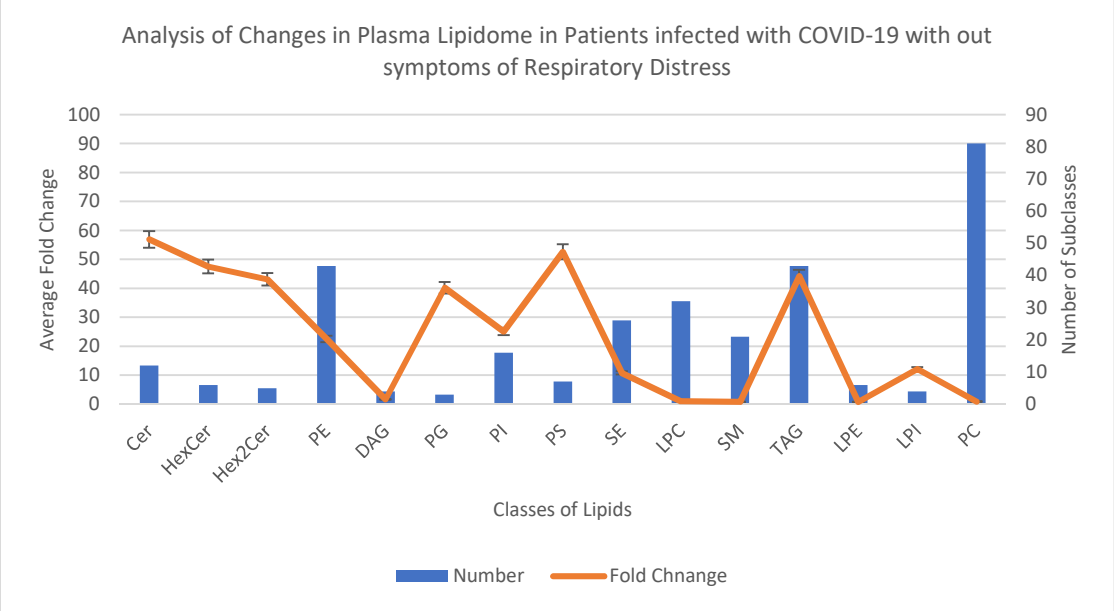

Figure 4b

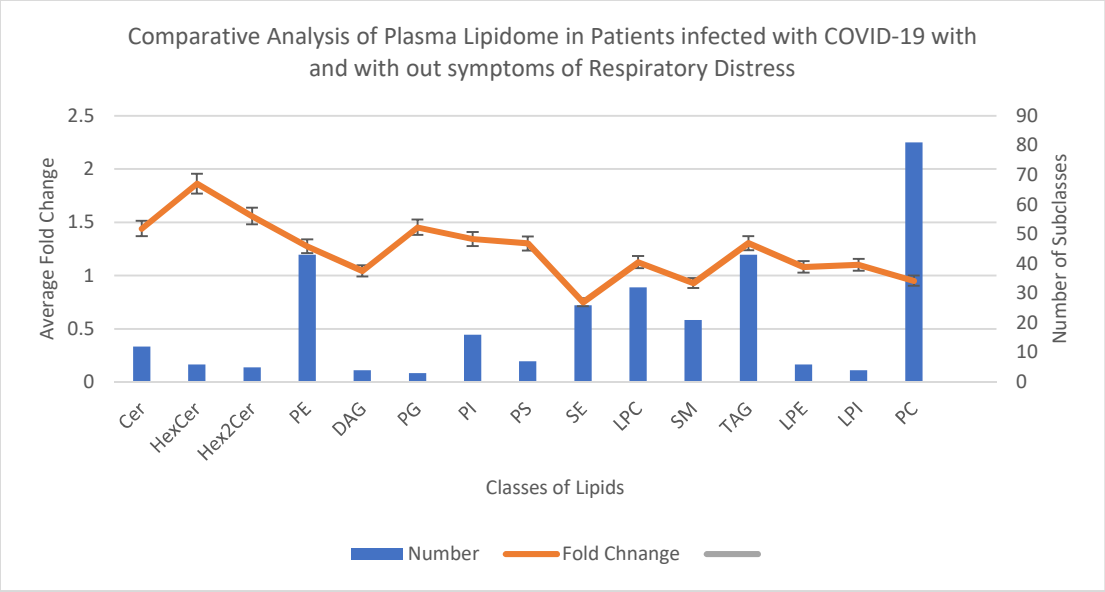

Figure 4c

Figure 4. Effect of Covid-19 infection on Plasma Lipidome

Number of subclasses identified per lipid class in plasma of Covid-19 infected individuals, and fold sum of MEDM changes in peak areas of identified lipid classes between the non-infected and with **(A),** mild (**B),** with respiratory distress symptoms. **(C),** Comparative differences analysis of lipids with the lipidome of plasma in individuals with COVID-19 infection with mild vs respiratory distress symptoms.

Figure 5a

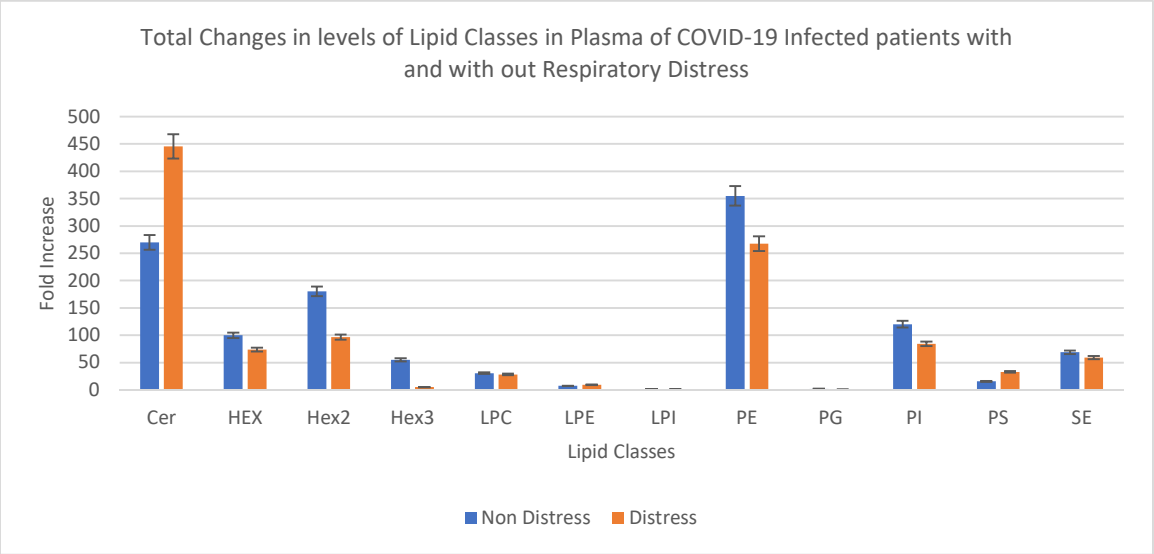

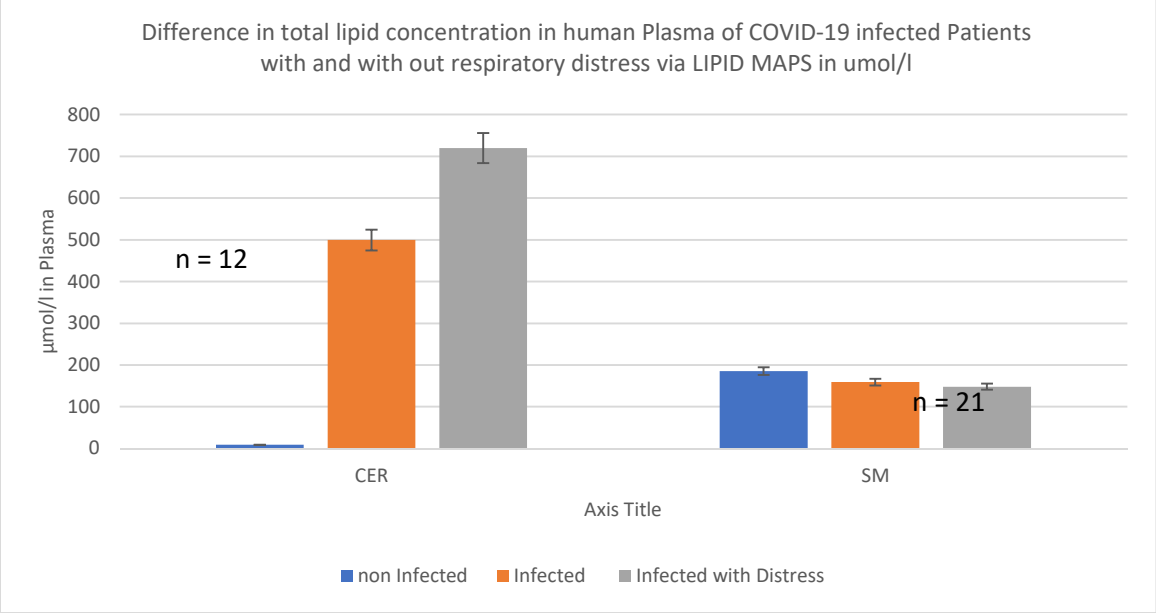

Figure 5b

Figure 5. Total Levels of Ceramide in Plasma of the Covid-19 infected

Fold sum of MEDM changes of peak area times number of subclasses identified per lipid class. **(A)** An overall estimation of relative changes in the concentrations of various lipid classes. **(B)** Relative concentration of lipids per class in µmoles/l of plasma as determined via the SRM 1950 consensus LIPID MAPS consortium.

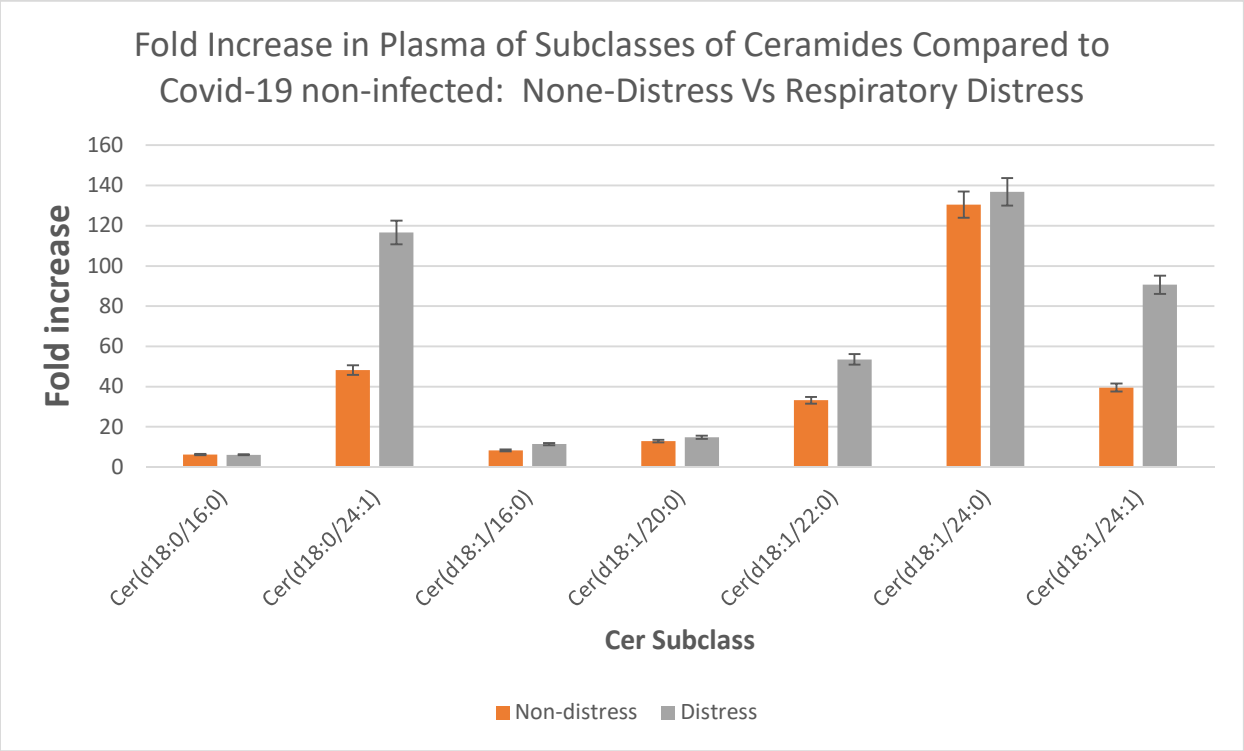

Figure 6a

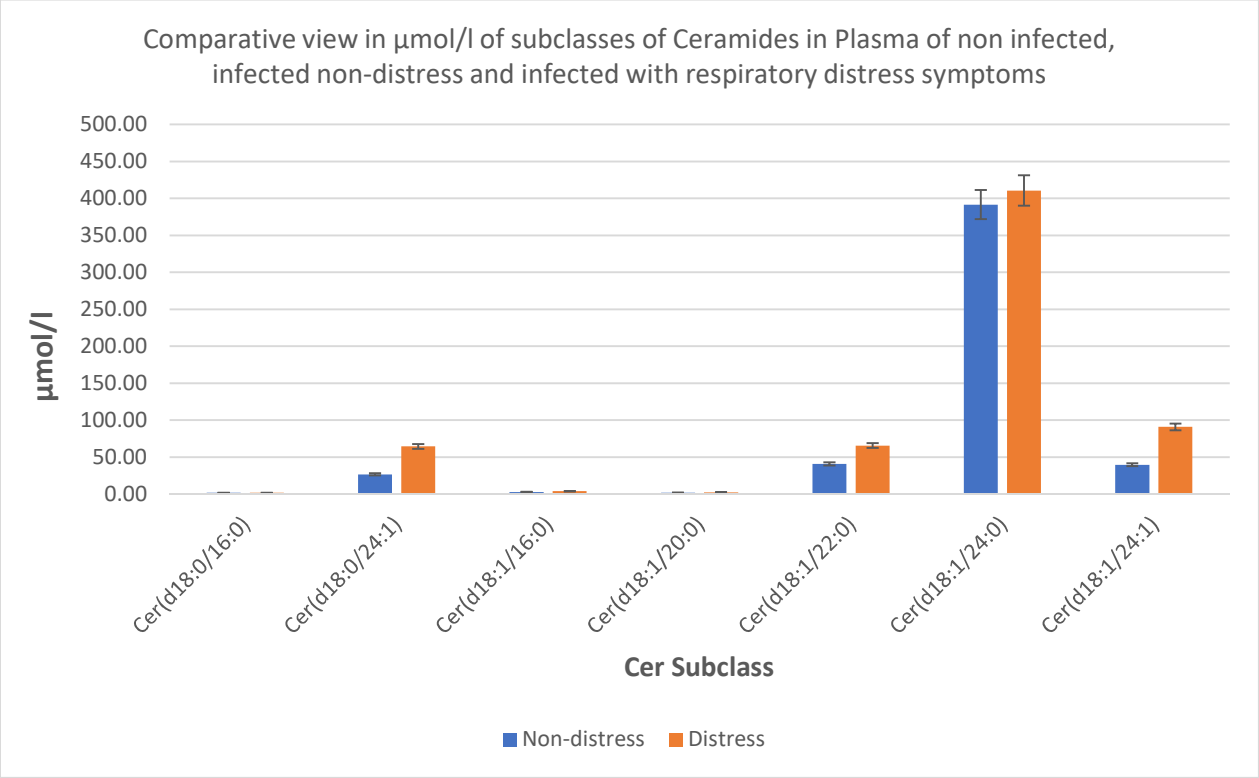

Figure 6b

Figure 6c

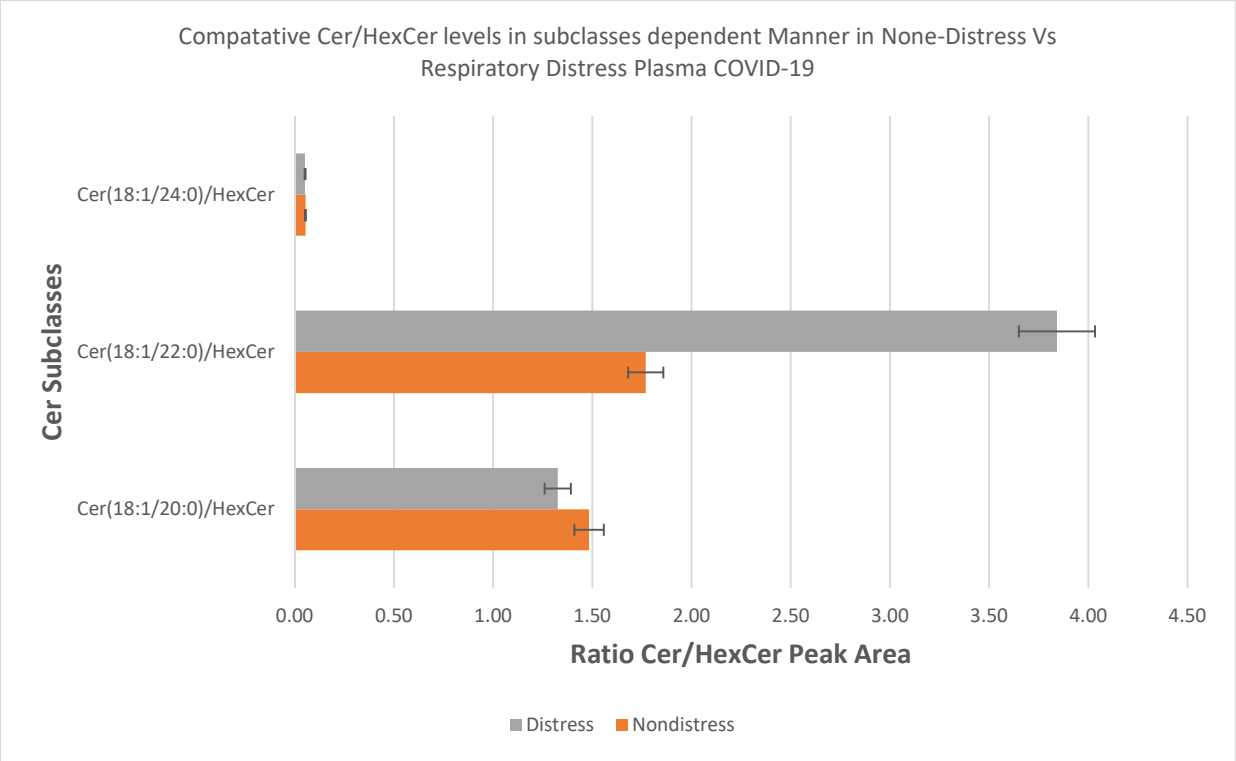
Compatative Cer/HexCer levels in subclasses dependent Manner in None-Distress Vs Respiratory Distress Plasma COVID-19
Cer Subclasses
Cer(18:1/24:0)/HexCer
Cer(18:1/22:0)/HexCer
Cer(18:1/20:0)/HexCer
0.00
0.50
1.00
1.50
2.00
2.50
3.00
3.50
4.00
4.50
Ratio Cer/HexCer Peak Area
Distress
Nondistress

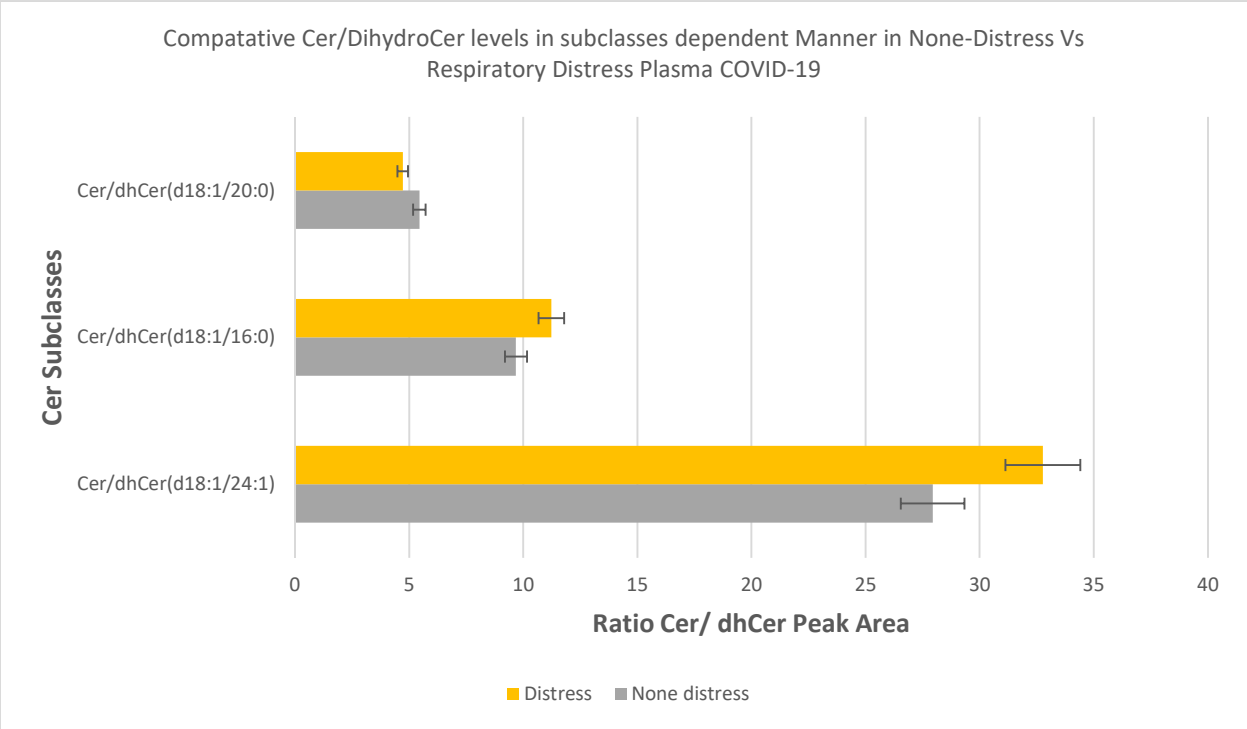
Compatative Cer/DihydroCer levels in subclasses dependent Manner in None-Distress Vs Respiratory Distress Plasma COVID-19
Cer Subclasses
Cer/dhCer(d18:1/20:0)
Cer/dhCer(d18:1/16:0)
Cer/dhCer(d18:1/24:1)
0
5
10
15
20
25
30
35
40
Ratio Cer/ dhCer Peak Area
Distress
None distress

Figure 6d

Figure 6. Ratios of lipids as predictive tests for respiratory distress

Comparative abundance profile of the identified subclasses of ceramides and **(A)** fold changes in observed peak area, compared to the plasma of uninfected individuals, of each identified ceramide subclass in terms of its relative abundance in the plasma of COVID-19 patients infected with mild and respiratory distress symptoms. **(B)** Comparative view, in μmol/l, of subclasses of ceramides in the plasma of noninfected, COVID-19-infected nondistress and respiratory distress symptoms. **(C)** Relative abundance profile as represented by the ratio of peak areas of ceramide/HexCer and ceramide/dihydroceramide levels (D) in a subclass-dependent manner in the plasma of COVID-19 patients infected with non-distress vs respiratory distress symptoms.

Supplementary Files

This is a list of supplementary files associated with this preprint. Click to download.

- Supplementaryfigures.pdf